ELSEVIER

Computers & Geosciences 33 (2007) 367–382

COMPUTERS & GEOSCIENCES

www.elsevier.com/locate/cageo

Joint inversion of AVA data for elastic parameters by bootstrapping

Hülya Kurt*

Istanbul Technical University, Department of Geophysics, 34390-Maslak, Istanbul, Turkey

Received 27 February 2006; received in revised form 24 August 2006; accepted 27 August 2006

Abstract

A joint inversion method is developed to estimate the elastic constants of two elastic, homogeneous, isotropic media separated by a flat horizontal boundary. The method jointly uses P and S-converted wave reflection amplitude-versus-angle (AVA) data and seeks the Poisson's ratios of each layer, ratios of the densities and bulk modulus of the layers. The generalized linear inversion (GLI) method is used as a mathematical tool and the Zoeppritz equations defining the seismic energy partitioning at a boundary are used as the physical model.

The P and S-converted wave velocity terms in the Zoeppritz equations were replaced by the bulk modulus (k_1, k_2), Poisson's ratios (σ_1, σ_2), and densities (ρ_1, ρ_2) of each layer. After expressing the equations in these six elastic constants, reflection coefficients of P and S-converted waves (R_{pp}, R_{ps}) are obtained as functions of ratios of bulk modulus and densities of the lower layer to those of the upper layer (k_2/k_1 and ρ_2/ρ_1) and Poisson's ratios of the upper and lower layers (σ_1 and σ_2). Using the ratios of bulk modulus and densities, the number of unknown parameters is reduced from 6 to 4 and this improves the success of inversion. The other contribution is that the calculation of R_{pp} and R_{ps} and their derivatives with respect to elastic constants and their ratios in the inversion are calculated analytically and coded in the Fortran programming language. In this way, the approach has an important advantage among the other AVA inversion methods, which are mostly based on numerical solutions or approximations to the Zoeppritz equations. A bootstrapping method of statistical analysis is combined with the GLI method to find the most likely elastic parameters and their confidence limits for repeated inversions for a large number of times by rearranging the noise distribution of the AVA data.

Keywords: AVA; Joint inversion; Elastic parameters; Bootstrapping; Zoeppritz equations

1. Introduction

Variation of seismic reflection and transmission coefficients with angle of incidence has been widely investigated to extract information about the lithology and subsurface elastic parameters (Ostrander, 1984; Backus, 1987; Rutherford and Williams, 1989). Seismic amplitude-versus-offset (AVO) and amplitude-versus-angle (AVA) data contain information about the elastic parameters of the subsurface. The Zoeppritz equations describe the reflection and transmission coefficients for plane waves as a function of incidence angle and six independent seismic parameters (P and S wave velocities, and density of the upper and lower media) (Berkhout, 1987). The equations were developed by Zoeppritz (1919), described in matrix form by Aki and

*Tel.: +90 212 2856255; fax: +90 212 2856201.
E-mail address: kurt@itu.edu.tr.

0098-3004/$ - see front matter © 2006 Elsevier Ltd. All rights reserved.
doi:10.1016/j.cageo.2006.08.012

Richards (2002) and their various analytic approximate forms are published in the literature (Bortfeld, 1961; Shuey, 1985). Lavaud et al. (1999), reparameterize the full equation in terms of a background and three contrasting parameters and use singular value decomposition analysis to study information content of P and P-converted S-wave AVO data.

Inversion of seismic AVO/AVA data for physical properties that enables direct lithological interpretation has been applied to the estimation of elastic parameters especially in reservoir rocks. AVO/AVA inversion can be performed either in the x–t domain (Dahl and Ursin, 1992; Mahob et al., 1999) or in the τ–p domain (Carazzone and Srnka, 1993; Buland et al., 1996). Linear or nonlinear approaches of AVO/AVA inversion methods can be carried out in either 2 dimensions (2D) or 3 dimensions (3D). The linearized inversion of 2D AVO data in x–t domain is performed to find P-wave velocities, S-wave velocities and density ratios of two-layered horizontal models (Demirbağ et al., 1993). In their study, the most likely solutions and confidence limits are estimated by a bootstrapping method. A Bayesian approach is also used in AVO inversion studies with probabilistic estimates of the unknown parameters from uncertain data and apriori information. Nonlinear inversion of AVO data by the Bayesian formulation provides the estimates of uncertainties of the viscoelastic physical parameters at an interface (Riedel et al., 2003). A 3D linearized AVO inversion method in a Bayesian framework with spatially coupled model parameters is developed to obtain posterior distributions for P-wave, S-wave velocity and density (Buland et al., 2003).

Joint analysis and inversion of reflected P-waves (PP) and S-converted waves (PS) in AVO/AVA data should provide better estimates of elastic parameters when compared with the standard P-wave approach alone. A practical method for the joint inversion of PP and PS reflection coefficients is described and applied to field data in the study of Margrave et al. (2001). The results from joint inversion are better because the ambiguities in the PP-only data are reduced. Various data sets are also used for inversion of AVO, e.g., a joint AVO inversion procedure of seismic data and well-log data are used to estimate P-wave, S-wave velocity and density as well as seismic wavelet and seismic-noise level (Buland and More, 2003). Both travel times and amplitudes are jointly used in the inversion to find elastic parameters at the reflectors (Wang, 1999; Buland and Landrø, 2001).

Estimation of rock properties (elastic moduli) directly from AVO data may give more physical insights than classical parameters of P and S velocities, and density. For example, Young's modulus is an appropriate modulus for describing the effects of pressure upon rock properties. Pigott et al. (1989) have suggested that this elastic constant can be dynamically determined from the inversion of AVO data. Stewart et al. (1995) show that Lame parameters (λ-compressibility and μ-shear) of the medium better differentiate rock properties. Similarly, a joint inversion AVA study by Goodway et al. (1997) shows that λ, μ and λ/μ parameters are more sensitive to changes in rock properties than P and S wave velocities (V_p and V_s) and V_p/V_s. Estimation of rock properties such as lithology, porosity, and pore fluid content are needed for quantitative extraction of rock properties by AVO analysis. The bulk modulus of the rocks (k, rock incompressibility), which defines the ratio of volumetric stress to volumetric strain, is strongly dependent on the pore fluid of rocks (Domenico, 1977). Poisson's ratio has a strong influence on changes in reflection coefficient as a function of incidence angle. Theory and laboratory measurements indicate that high-porosity gas sands tend to exhibit abnormally low Poisson's ratios (Ostrander, 1984). Density contrasts give important information about the lithology or the fluid saturation of the reservoir.

In this paper, a technique is developed to perform a joint AVA inversion of P and S-converted waves from prestack seismic reflection data. The method estimates the ratios of bulk moduli (r_k) and density (r_ρ) of the lower layer to those of the upper layer (k_2/k_1 and ρ_2/ρ_1) and Poisson's ratios of the upper and lower layers (σ_1 and σ_2) of two elastic medium separated by a horizontal boundary. Because bulk moduli and density contrasts and Poisson's ratio are sensitive to lithology, porosity and pore fluid contents of rocks that affect seismic amplitudes, these elastic constants are chosen as model parameters along with densities. The number of unknown parameters in the inversion procedure decreases from 6 to 4 by taking the contrasts of the bulk moduli and densities rather than individual values of k_1, k_2, ρ_1, ρ_2. The full form of the P and S wave reflection coefficients are expressed analytically in linear equation systems from the Zoeppritz equations. Moreover, the derivatives of R_{pp} and R_{ps} with respect to the unknown parameters of the Jacobian matrix are formed analytically providing an increase in the sensitivity and reliability of the inversion. Amplitudes are normalized to the values

of the first angle, i.e., 1° ($R_{pp}(1)$ and $R_{ps}(1)$) instead of 0° as in traditional AVO/AVA studies. This is done in order to avoid uncertainty in the analytical computation of the Jacobian derivatives at zero degree angle of incidence of reflections. The expressions of R_{pp} and R_{ps} are nonlinear functions of the searched parameters r_k, r_ρ, σ_1 and σ_2. Residual function maps (RFM) (Demirbağ et al., 1993) are used to investigate the degree of nonlinearity in the generalized inversion method. Statistically significant mean values and standard deviations to be used as inputs in inverse simulations were generated from a database using a bootstrapping method (Efron and Gong, 1983). Two reservoir models are used to test the inversion method and results are enhanced by the bootstrapping and compared for the presence of random noise.

1.1. The Zoeppritz equations as functions of elastic parameters

The physical model of this study is the Zoeppritz equations, which describes the energy partitioning at an interface when an obliquely incident plane *P*-wave impinges on this interface for pre-critical angles. Two semi-infinite, homogeneous, isotropic elastic media separated by a horizontal plane interface are assumed for deriving the equations (Zoeppritz, 1919; Aki and Richards, 2002). The parameters of the classical form of the Zoeppritz equations are *P* and *S* wave velocities ($V_{p1}, V_{s1}, V_{p2}, V_{s2}$) and densities ($\rho_2, \rho_1$) of each layer, *P* and *S* wave reflection and transmission angles ($\theta_r, \Phi_r, \theta_t \Phi_t$), *P* wave incident angle ($\theta_1 = \theta_r$), and reflection and transmission coefficients of *P* and *S* waves ($R_{pp}, R_{ps}, T_{pp} T_{ps}$).

Some substitutions were carried out to convert the equations from the classical form to the new form with the chosen elastic constants. In the new form, V_p and V_s of each layer are written in terms of elastic constants; density (ρ), bulk moduli (k) and Poisson's ratio (σ) (Sheriff and Geldart, 1995).

$$V_{p1} = \left[\frac{3k_1(1-\sigma_1)}{\rho_1(1+\sigma_1)}\right]^{1/2}, \quad V_{p2} = \left[\frac{3k_2(1-\sigma_2)}{\rho_2(1+\sigma_2)}\right]^{1/2},$$

$$V_{s1} = \left[\frac{3k_1(1-2\sigma_1)}{2\rho_1(1+\sigma_1)}\right]^{1/2}, \quad V_{s2} = \left[\frac{3k_2(1-2\sigma_2)}{\rho_2(1+\sigma_2)}\right]^{1/2}. \tag{1}$$

In Eqs. (1), the upper medium is designated by subscript "1" and the lower medium by "2". By using Eqs. (1), the new form of the Zoeppritz equations with elastic constants is obtained as follows:

$$\begin{bmatrix} \sin\theta_1 & \cos\phi_r & -\sin\theta_t & \cos\phi_t \\ -\cos\theta_1 & \sin\phi_r & -\cos\theta_t & -\sin\phi_t \\ \sin(2\theta_1) & \cos(2\phi_r)\left[\frac{1-\sigma_1}{0.5-\sigma_1}\right]^{1/2} & \sin(2\theta_t)\left[\frac{\rho_2 k_2(1-\sigma_1)(1+\sigma_1)}{\rho_1 k_1(1-\sigma_2)(1+\sigma_2)}\right]^{1/2}\left[\frac{1-2\sigma_2}{1-2\sigma_1}\right] & -\cos(2\phi_t)\left[\frac{\rho_2 k_2 2(1-2\sigma_2)(1-\sigma_1)}{\rho_1 k_1\ (1+\sigma_2)(1+\sigma_1)}\right]^{1/2}\left[\frac{1+\sigma_1}{1-2\sigma_1}\right] \\ \cos(2\phi_r) & -\sin(2\phi_r)\left[\frac{0.5-\sigma_1}{1-\sigma_1}\right]^{1/2} & -\cos(2\phi_t)\left[\frac{\rho_2 k_2(1-\sigma_2)(1+\sigma_1)}{\rho_1 k_1(1+\sigma_2)(1-\sigma_1)}\right]^{1/2} & -\sin(2\phi_t)\left[\frac{\rho_2 k_2(1-2\sigma_2)(1+\sigma_1)}{\rho_1 k_1 2(1+\sigma_2)(1-\sigma_1)}\right]^{1/2} \end{bmatrix} \times \begin{bmatrix} R_{pp} \\ R_{ps} \\ T_{pp} \\ T_{ps} \end{bmatrix} = \begin{bmatrix} -\sin\theta_1 \\ -\cos\theta_1 \\ \sin(2\theta_1) \\ -\cos(2\phi_r) \end{bmatrix}. \tag{2}$$

Note that in the new form of the Zoeppritz equations, the densities and bulk moduli are in the ratios of the lower layer to the upper layer. Therefore, $r_\rho = \rho_2/\rho_1$, $r_k = k_2/k_1$, σ_1 and σ_2 can be defined as new variables which are the model parameters of the inversion procedure where the independent variable (controlled parameter) is θ_1.

Using Snell's law, reflection and transmission angles of *P* and *S* waves in the new form of the Zoeppritz equations are also written as functions of

these elastic constants:

$$\theta_t = \arcsin\left\{\left(r_k r_\rho \frac{(1-\sigma_2)(1+\sigma_1)}{(1+\sigma_2)(1-\sigma_1)}\right)^{1/2}\sin\theta_1\right\},$$

$$\phi_r = \arcsin\left\{\left(\frac{0.5-\sigma_1}{1-\sigma_1}\right)^{1/2}\sin\theta_1\right\},$$

$$\phi_t = \arcsin\left\{\left(\frac{r_k}{r_\rho}\frac{(1-2\sigma_2)(1+\sigma_1)}{2(1+\sigma_2)(1-\sigma_1)}\right)^{1/2}\sin\theta_1\right\}. \quad (3)$$

Expressing Eq. (2) with the new arrangements involved in Eqs. (3), the parameterization of P and S-wave reflection coefficients can be written as

$$R_{pp} = f(r_\rho, r_k, \sigma_1, \sigma_2, \theta_1),$$

$$R_{ps} = f(r_\rho, r_k, \sigma_1, \sigma_2, \theta_1) \quad (4)$$

in the Appendix. Analytical expressions of R_{pp} and R_{ps} are used for forward modeling and they constitute a base for the inversion procedure. By proper arrangements of R_{pp} and R_{ps}, many parts in the equations appearar in identical form that enables easy Fortran coding.

1.2. Inversion of AVA data and bootstrapping

The model parameters can be obtained by inverse solution of the new form of the Zoeppritz equations. The data are P and S-converted wave reflection coefficients (R_{pp} and R_{ps}) as a function of incident angle (θ_1), which is defined as the controlled parameter of the inversion. The new form of the Zoeppritz equations with the elastic parameters, as given in the Appendix, is taken as the forward model. The equations are nonlinear functions of model parameters r_ρ, r_k, σ_1 and σ_2, thus they can be approximated by a first order Taylor series expansion to form a set of linear equations as follows:

$$R_i = R_i(p^0) + \sum_{j=1}^{n}\left.\frac{\partial R_i}{\partial p_j}\right|_{p=p^0}(p_j - p_j^0), \quad (5)$$

where R_i represents the perturbation of the model response about the initial model parameters, p^0 are the initial model parameters, $R_i(p^0)$ are the computed reflection coefficients from the initial model parameters and n is the number of observations. The damped least squares solution (Marquardt–Levenberg) method is taken as the mathematical tool for solving the inversion (Lines and Treitel, 1984). The parameter change vector (Δp) in the generalized linear inversion (GLI) method is as follows:

$$\Delta p = (J^T J + \beta I)^{-1} J^T \Delta R, \quad (6)$$

where ΔR denotes the difference between the observed and the initial model data; J, the Jacobian matrix; β, Marquardt factor and I, identity matrix. Iterated values of the parameters can be found from

$$p = \Delta p + p^0, \quad (7)$$

where "p" is the iterated value and p^0 is the initial value. The Jacobian matrix (J) as given in Eq. (8) contains the derivatives of the P and S-converted wave reflection coefficients with respect to the model parameters r_ρ, r_k, σ_1, σ_2. If only R_{pp} or R_{ps} data sets are used in the inversion, the Jacobian matrix would have derivatives of R_{pp} or R_{ps} individually. In the joint inversion case, the Jacobian matrix has derivatives of two data sets (R_{pp} and R_{ps}) yielding a $(2\times n)\times m$ dimensional matrix where n is the number of observations and m is the number of the unknown parameters. The value of m is 4 and n is the integer number of the observation angles of the two horizontal layer model.

parameter

$$J = \begin{bmatrix}
\left.\frac{\partial Rpp}{\partial r_\rho}\right|_{\theta_1=\theta_1^1} & \left.\frac{\partial Rpp}{\partial r_k}\right|_{\theta_1=\theta_1^1} & \left.\frac{\partial Rpp}{\partial \sigma_1}\right|_{\theta_1=\theta_1^1} & \left.\frac{\partial Rpp}{\partial \sigma_2}\right|_{\theta_1=\theta_1^1} \\
\left.\frac{\partial Rpp}{\partial r_\rho}\right|_{\theta_1=\theta_1^2} & \left.\frac{\partial Rpp}{\partial r_k}\right|_{\theta_1=\theta_1^2} & \left.\frac{\partial Rpp}{\partial \sigma_1}\right|_{\theta_1=\theta_1^2} & \left.\frac{\partial Rpp}{\partial \sigma_2}\right|_{\theta_1=\theta_1^2} \\
\vdots & \vdots & \vdots & \vdots \\
\left.\frac{\partial Rpp}{\partial r_\rho}\right|_{\theta_1=\theta_1^n} & \left.\frac{\partial Rpp}{\partial r_k}\right|_{\theta_1=\theta_1^n} & \left.\frac{\partial Rpp}{\partial \sigma_1}\right|_{\theta_1=\theta_1^n} & \left.\frac{\partial Rpp}{\partial \sigma_2}\right|_{\theta_1=\theta_1^n} \\
\left.\frac{\partial Rps}{\partial r_\rho}\right|_{\theta_1=\theta_1^1} & \left.\frac{\partial Rps}{\partial r_k}\right|_{\theta_1=\theta_1^1} & \left.\frac{\partial Rps}{\partial \sigma_1}\right|_{\theta_1=\theta_1^1} & \left.\frac{\partial Rps}{\partial \sigma_2}\right|_{\theta_1=\theta_1^1} \\
\left.\frac{\partial Rps}{\partial r_\rho}\right|_{\theta_1=\theta_1^2} & \left.\frac{\partial Rps}{\partial r_k}\right|_{\theta_1=\theta_1^2} & \left.\frac{\partial Rps}{\partial \sigma_1}\right|_{\theta_1=\theta_1^2} & \left.\frac{\partial Rps}{\partial \sigma_2}\right|_{\theta_1=\theta_1^2} \\
\vdots & \vdots & \vdots & \vdots \\
\left.\frac{\partial Rps}{\partial r_\rho}\right|_{\theta_1=\theta_1^n} & \left.\frac{\partial Rps}{\partial r_k}\right|_{\theta_1=\theta_1^n} & \left.\frac{\partial Rps}{\partial \sigma_1}\right|_{\theta_1=\theta_1^n} & \left.\frac{\partial Rps}{\partial \sigma_2}\right|_{\theta_1=\theta_1^n}
\end{bmatrix}$$

Number of observations

$(2xn)$ x m . (8)

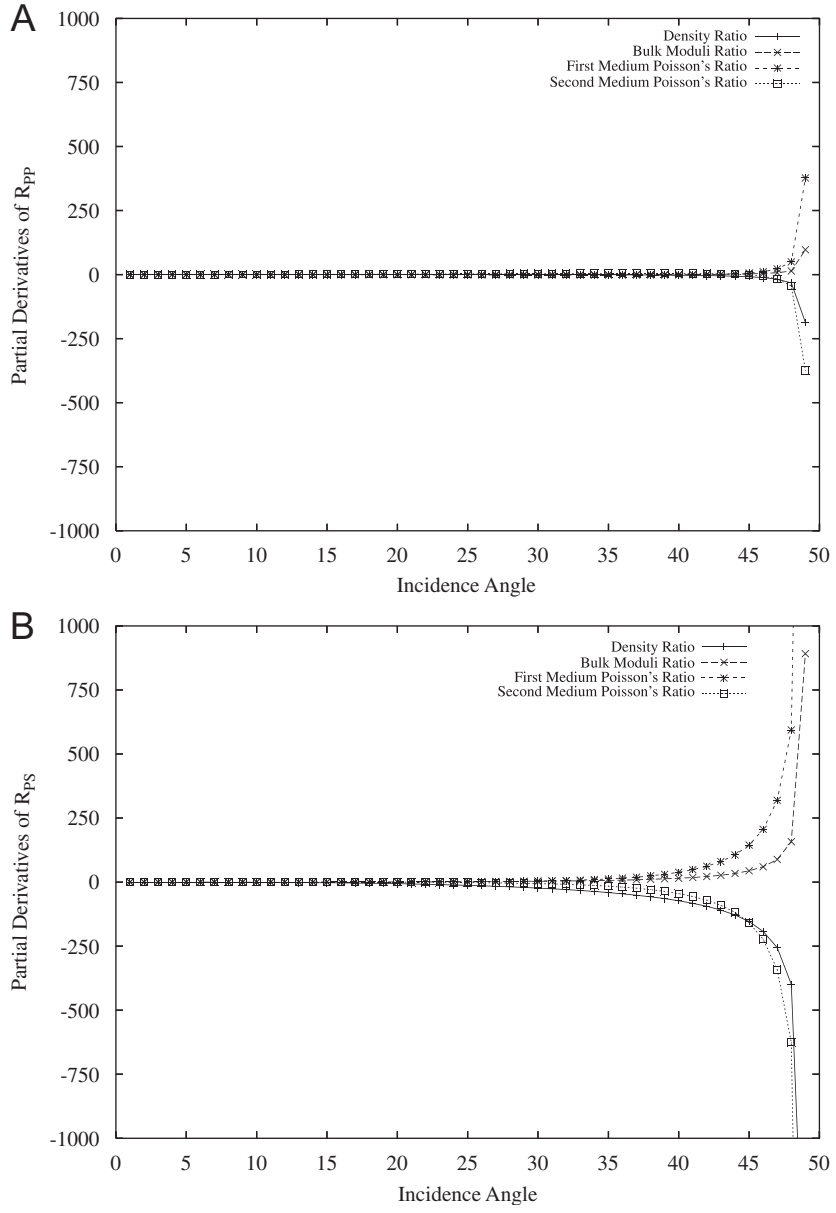

Fig. 1. Graphs of derivatives of R_{pp} and R_{ps} with respect to elastic parameters for shale/limestone (gas) interface model with $r_\rho = 1.04$, $r_k = 1.86$, $\sigma_1 = 0.23$, $\sigma_2 = 0.24$.

In this inversion procedure, the derivatives in the Jacobian matrix (J) are taken analytically to achieve precise computation. The partial derivatives are evaluated for each value of the controlled parameter (θ_1) from zero to the critical angles of incidence. The curves obtained by the evaluation of the partial derivatives of R_{pp} and R_{ps} as a function of incidence angle (θ_1), are given in Fig. 1A and B. The partial derivatives of R_{pp} and R_{ps} with respect to the model parameters are calculated for a two layered shale/limestone (gas) interface test model with $r_\rho = 1.04$, $r_k = 1.86$, $\sigma_1 = 0.23$ and $\sigma_2 = 0.24$ (Dey-Sarkar and Svatek, 1993). The derivatives are calculated from zero to critical angle (49°) of incidence with an increment of 1°. For illustration of R_{pp} and R_{ps}, the same scale is used for the vertical axis to compare partial derivative variations for each elastic parameter. Notice that derivative curves in Fig. 1A and

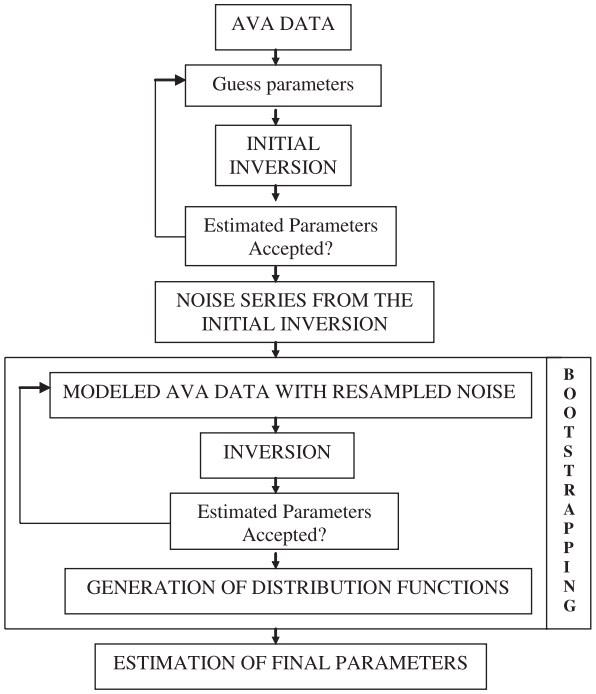

Fig. 2. Flowchart of inversion method.

B change continuously and smoothly indicating that inversion procedure can be carried out free of problems. Derivatives have adequate change range in the pure R_{ps} case but not in the pure R_{pp} case. That is to say, if only R_{pp} data are used in the inversion procedure, results would not be satisfactory. A large amount of variation occurs at the position close to the critical angle for both R_{pp} and R_{ps} derivative graphics. This shows that the data must have as wide angles as possible.

As seen in the flowchart of the inversion procedure in Fig. 2, synthetic AVA data and initial guess parameters are provided to the GLI to get an initial solution vector satisfying the preset physical constraints. The probable values of physical constraints are changing from 0.25 to 1.5 for density ratio, from 0.25 to 4.0 for bulk moduli ratio and from 0.05 to 0.45 for Poisson's ratios. This initial section of the inversion procedure produces initial elastic parameters and provides a basis to calculate a model AVA response.

The noise series obtained from the differences between model AVA response and AVA synthetic data are added onto the model response to simulate new AVA data. The effect of random noise in the inversion by the GLI method is unpredictable. Therefore, the resulting solutions for the elastic parameters can be considered as random variables around the true elastic parameters. If the data acquisition had been repeated many times, the random noise on the data would have been different. In practice, computers are used to simulate the data acquisition many times by resampling the random noise from the original data. The simulated AVA data with resampled noise are again inverted to find a solution vector that satisfies the preset physical constraints. The inversion algorithm is coupled with a bootstrapping statistical technique (Efron and Gong, 1983; Efron and Tibshirani, 1993) to find the most likely parameters and their confidence limits. As seen in Fig. 2, the basic inversion is repeated for a large number of times by rearranging the noise distribution of the AVA data. If the inverted elastic parameters satisfy the predefined mathematical and physical constraints, they are stored. When a predetermined number of solution vectors are obtained (in this study it is used a range of 1000–10 000) the stored elastic parameters are used to generate the frequency histograms from which the most likely elastic parameters and their confidence limits can be determined. Statistically reasonable values and standard deviations, used as an input to the simulations, were generated from accumulated solutions using the bootstrapping method.

1.3. Linearity and uniqueness of the inversion

The Zoeppritz equations, which are the physical model of the inversion procedure, are nonlinear functions of model parameters r_ρ, r_k, σ_1, σ_2 as in the Appendix. The equations are approximated by a first order Taylor series expansion to form a set of linear equations. The linearity and uniqueness of the inversion problem for seismic amplitude data were investigated by generating RFM (Demirbağ et al., 1993; Larsen, 1999) for a variety of models. The residual error function (E_{ps}) for the joint use of the R_{pp} and R_{ps} data sets which are defined for selected parameter pairs (k, l) is given as below:

$$E_{ps}(k,l) = \sum_{i=1}^{N} \{R_{m-pp} - R_{pp}(k,l)\}^2 + \sum_{i=1}^{N} \{R_{m-ps} - R_{ps}(k,l)\}^2, \quad (9)$$

where R_{m-pp} and R_{m-ps} are forward model response of the chosen values of the model parameters (R_{pp}

and R_{ps} values from the Zoeppritz equations). $R_{pp}(k,l)$ and $R_{ps}(k,l)$ are the response of the same function to different values of the desired parameter pair (k,l). $E_{ps}(k,l)$ is evaluated for all incidence angles from 0 to N, where N is the critical angle of incidence. RFMs having closed contours with one minimum imply a unique solution, that is to say, a non-linear function can be formulated in a GLI

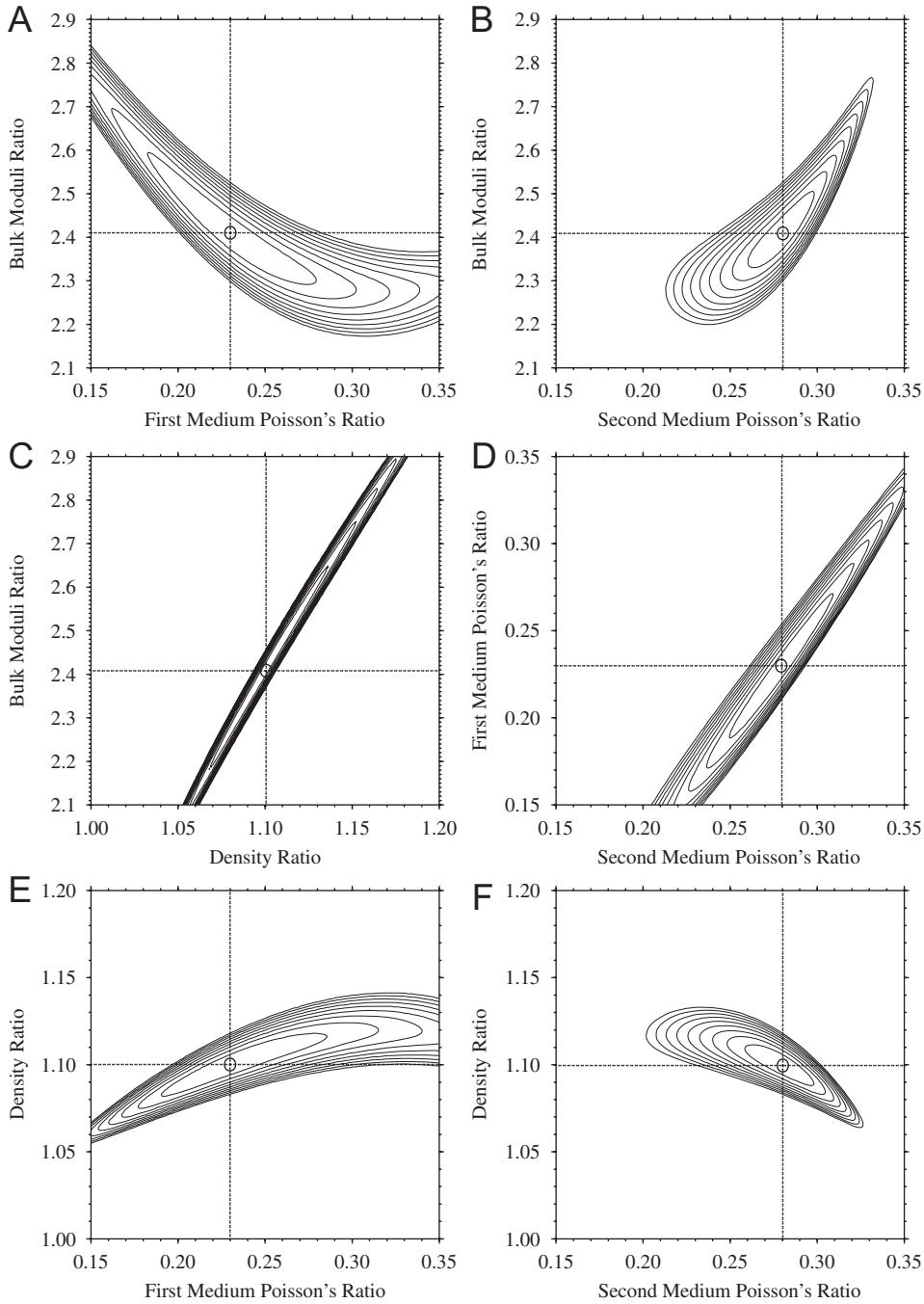

Fig. 3. Residual function maps of shale/limestone model for r_k–σ_1, r_k–σ_2, r_k–r_ρ, σ_2–σ_1, r_ρ–σ_1, r_ρ–σ_2 parameter pairs. R_{pp} and R_{ps} data sets are used to produce residual errors. Contour values change from 0.01 to 0.1 by increments of 0.01. Crossing vertical and horizontal dotted lines having a circle at crossing point mark actual values of model parameters.

scheme by two-term Taylor series expansion. The RFMs for the model parameters of P and S velocities (V_p, V_s) and densities (ρ) of two-layered horizontal interface models were studied using only the P wave data case as in Demirbağ et al. (1993) and P and S-converted wave reflection coefficients data simultaneously as in Larsen (1999). Their inversion procedures have five searched parameters for the two-layered earth model ($V_{p1}, V_{s1}, V_{p2}, V_{s2}$ and ρ_2/ρ_1) and they prepared RFMs for 10 combinations of parameter pairs.

The inversion method in this study has four model parameters; therefore, there are six combinations of parameter pairs to constitute the RFM. These are for r_k–σ_1, r_k–σ_2, r_k–r_ρ, σ_1–σ_2, r_ρ–σ_1 and r_ρ–σ_2 parameter pairs. RFMs are investigated for the shale/limestone interface model with $r_\rho = 1.1$, $r_k = 2.41$, $\sigma_1 = 0.23$ and $\sigma_2 = 0.28$ as in Fig. 3. Forward model responses of R_{pp} and R_{ps} values (R_{m-pp} and R_{m-ps} in Eq. (9)) for the test model are calculated analytically from the equations in the Appendix. Although the values of R_{m-pp} and R_{m-ps} should be calculated from 1° to the critical angle of incidence (45°), which is the maximum angle of the shale/limestone model, the maximum angle is chosen from minimum values of critical angles of incidences for each different model response value. $R_{pp}(k,l)$ and $R_{ps}(k,l)$ values are also calculated analytically from R_{pp} and R_{ps} as in the Appendix. Because the normalized values of R_{pp} and R_{ps} data are used in the inversion procedure, residual functions are also formed with the normalized reflection coefficients of P and S-converted waves as shown in Fig. 3 for r_k–σ_1, r_k–σ_2, r_k–r_ρ, σ_1–σ_2, r_ρ–σ_1, r_ρ–σ_2 parameter pairs.

Using known model parameters, the residual error function $E_{ps}(k,l)$ can be calculated for varying r_ρ, r_k, σ_1 and σ_2. As an example, amplitude responses of varying r_k and σ_1 around their actual values $(r_k = 2.41, \sigma_1 = 0.28)$ while r_ρ and σ_2 are constant at 1.1 and 0.28, respectively, is contoured as in Fig. 3A. The RFM for $(r_k - \sigma_1)$ parameter pairs shows elliptically closed contours around the actual parameters that are marked by crossing vertical and horizontal dotted lines. A well-defined minimum is also displayed for other parameter pairs of RFMs having contour values change from 0.01 to 0.1 by increments of 0.01 (from Fig. 3B to F). In the case of using only P reflection data for RFM, a long and wide valley is observed instead of closed

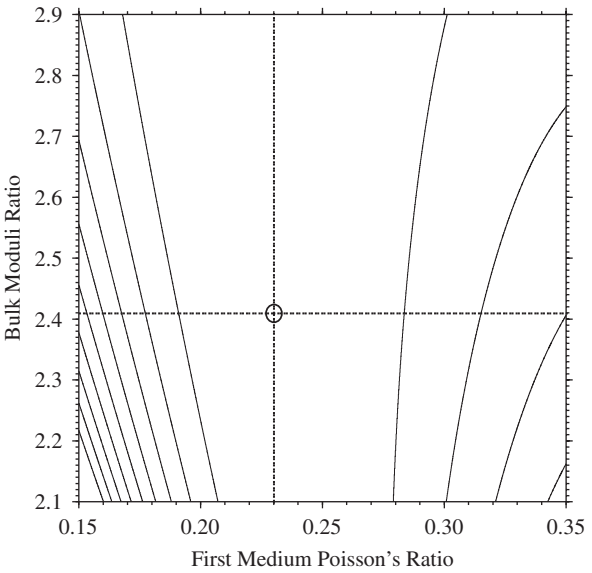

Fig. 4. Residual function maps of shale/limestone model for r_k–σ_1 parameter pairs. Only R_{pp} data set is used to produce residual errors. Contour values change from 0.01 to 0.1 by increments of 0.01. Crossing vertical and horizontal dotted lines having a circle at crossing point mark actual values of model parameters. Note that contours are not closed around exact value.

contours around the actual values for the RFM of $(r_k - \sigma_1)$ pairs (Fig. 4). This result is also inferred from R_{pp} and R_{ps} change graphics in the Fig. 5. Note that, R_{pp} variations as function of incidence angle are considerably smaller than R_{ps} variations for the shale/limestone interface model. Hence, using R_{ps} data with R_{pp} controls the contour closure around the actual parameter values in the RFMs as in Fig. 3. The RFM for P-wave reflections shows a poor degree of linearity between r_k and σ_1 and if the GLI method is used only with P reflections, inversion results would not be satisfactory. Similarly, Demirbağ et al. (1993) pointed out that RFMs have generally long and wide solution areas if σ_2 or σ_1 is used in a parameter pair with only R_{pp} data. Their reason for that is the absence of S-converted reflections, which are very effective on physical factors on Poisson's ratios. In this study, using both P and S-converted reflections for the σ_2–σ_1 parameter pair, the RFM displays a local single minimum with elliptically closed contours (Fig. 3D).

1.4. Examples of applications with test models

Various two-layer models were used to test the inversion method. Two of them that are also used

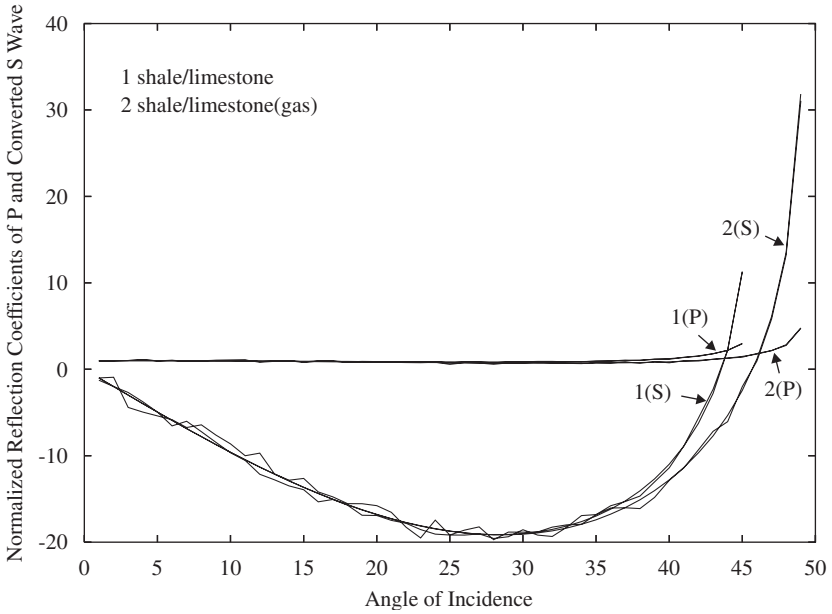

Fig. 5. Graphs of P and S-converted wave reflection coefficient series normalized to $R_{pp}(1^\circ)$ and $R_{ps}(1^\circ)$ for test models with 5% random noise.

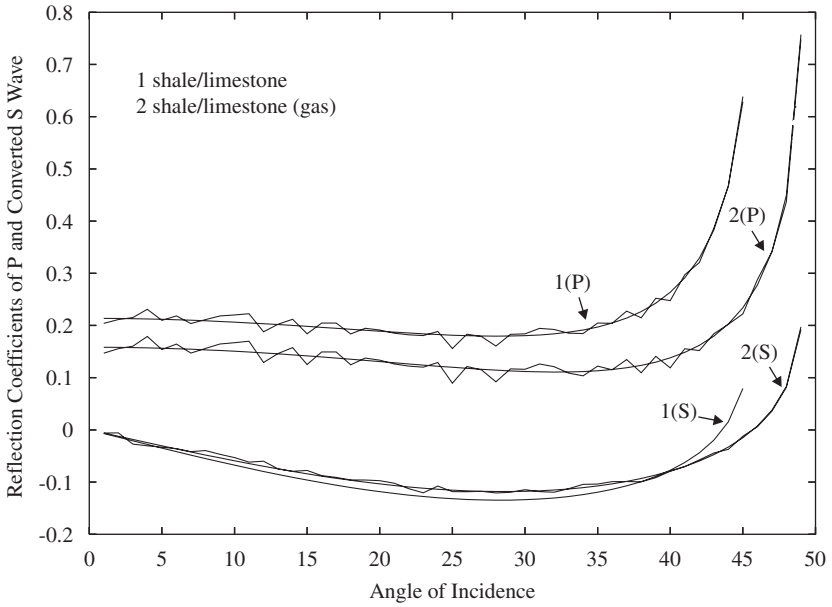

Fig. 6. Graphs of P and S-converted wave reflection coefficient series for test models with 5% random noise.

for investigating the partial derivatives and residual functions will be introduced here. These are the shale/limestone interface model with the $r_\rho = 1.1$, $r_k = 2.41$, $\sigma_1 = 0.23$ and $\sigma_2 = 0.28$ and the shale/limestone (gas) model with the $r_\rho = 1.04$, $r_k = 1.86$, $\sigma_1 = 0.23$ and $\sigma_2 = 0.24$ values. The typical values of P and S-wave velocities and the densities of layers are taken from Dey-Sarkar and Svatek (1993). Their values are used to find the values of model parameters using Eqs. (1). For the models, the upper medium is designated as shale while the lower layer is limestone and gas saturated limestone.

Although models are chosen from typical petroleum traps, the inversion code can be used for other types of earth layer units. R_{pp} and R_{ps} equations obtained from the Zoeppritz equations for precritical angles are used to produce a synthetic AVA data set for the models as in the Appendix. A random noise of 5% is added to each of the synthetic R_{pp} and R_{ps} data sets to simulate realistic amplitude data before introducing them to the inversion procedure. The synthetic AVA data for all the models are normalized to the $R_{pp}(1)$ and $R_{ps}(1)$ to get rid of the probable error effect of the exact values on the amplitudes. In Figs. 5 and 6, normalized and nonnormalized R_{pp} and R_{ps} reflection coefficients are displayed together as functions of the incidence angle from 1° to the critical angle of each model. *P* and *S*-converted wave reflection coefficients calculated from the Zoeppritz equations versus incidence angles of 1–45° (critical angle) for shale/limestone and 49° for shale/limestone (gas) models. Because the bulk moduli (k_2) and density (ρ_2) of the lower layers are larger than for the upper shale layer, the ratios of bulk moduli (r_k) and density (r_ρ) are larger than one. Note that when the ratios of bulk moduli and the density are larger than one, *P*-wave reflection coefficients have positive values and *S*-wave reflection coefficients have negative values (Figs. 5 and 6).

The GLI inversion procedure with bootstrapping is carried out as outlined in Fig. 2. The most likely elastic parameters for shale/limestone model are given in Fig. 7. The peak (mode) values (marked by central solid square on the horizontal axis) of the distribution functions are determined as the most

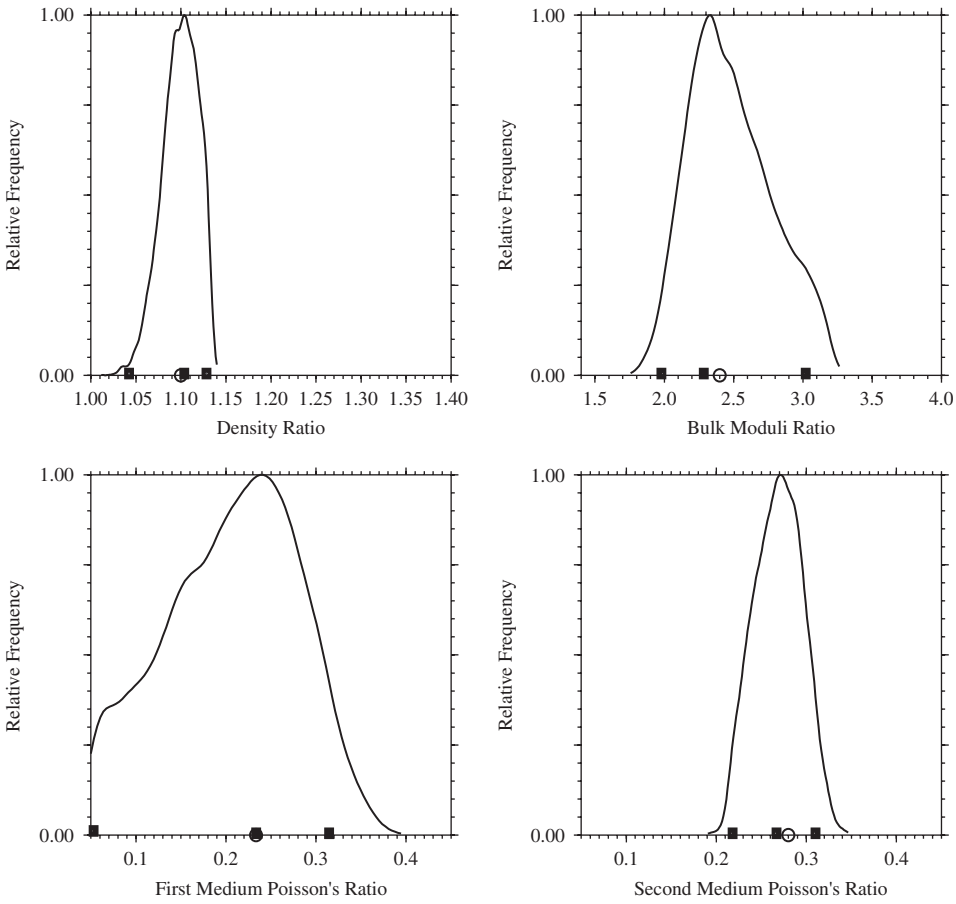

Fig. 7. Distribution functions of solutions for density ratio, bulk moduli ratio and Poisson's ratio of each layer for shale/limestone interface model used in inversion procedure. Solid square at peak value (mode) indicates the most likely parameters while squares on either side show 90% confidence limits of the most likely parameters. Open circle in horizontal axis shows actual value of elastic parameters ($r_\rho = 1.1, r_k = 2.41, \sigma_1 = 0.23, \sigma_2 = 0.28$).

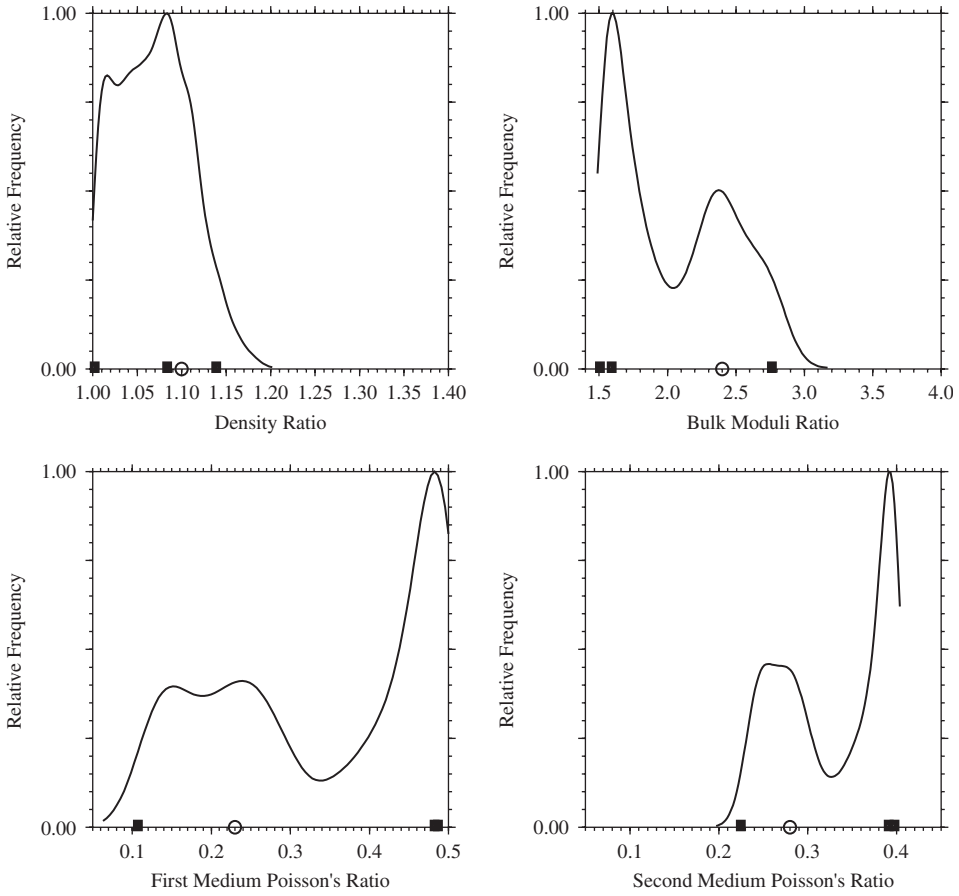

Fig. 8. Distribution functions of solutions for density ratio, bulk moduli ratio and Poisson's ratio of second layer for shale/limestone interface model if only P wave reflection coefficients are used in inversion procedure. Solid square at peak value (mode) indicates the most likely parameters while squares on either side show 90% confidence limits of the most likely parameters. Because peak value and maximum confidence limits of the most likely parameters are very close, solid squares are shown almost at same location for Poisson's ratios. Open circle in horizontal axis shows actual value of elastic parameters ($r_\rho = 1.1, r_k = 2.41, \sigma_1 = 0.23, \sigma_2 = 0.28$).

likely elastic parameters. An open circle on the horizontal axis of the graphics marks the actual parameters. For the shale/limestone interface model, distribution solutions show that inversion estimates are almost the actual parameters. Inversion results with $r_\rho = 1.101$, $r_k = 2.425$, $\sigma_1 = 0.225$ and $\sigma_2 = 0.278$ produce values that are very close to the original model parameters. The random noise level is chosen as 5% and initial parameters are 1.4, 1.9, 0.19, 0.18, for r_ρ, r_k, σ_1, σ_2, respectively. Joint use of R_{pp} and R_{ps} inversion results is more satisfactory then the R_{pp} only data for the same model. In this case, the density ratio is the only parameter that can be found satisfactorily with the same initial parameters, noise level and incidence angle value (Fig. 8). Results for shale/limestone (gas) model having 5% random noise give successful inversion solutions with $r_\rho = 1.045$, $r_k = 1.892$, $\sigma_1 = 0.216$ and $\sigma_2 = 0.232$ values (Fig. 9). The noise is added to data by taking the desired percentage noise level of the first value of the P and S-converted reflections. When the noise level in the shale/limestone (gas) model AVA data is increased from 5% to 7% and 10%, the inversion code can still find acceptable results. For example, with 10% noise the most likely solutions are found as $r_\rho = 1.008$, $r_k = 1.824$, $\sigma_1 = 0.243$ and $\sigma_2 = 0.242$. In this case, distributions of solutions give wide confidence limits especially for the Poisson's ratios. The inversion was performed between 1° to critical angles for the models. When the incidence angle limit is chosen as 30° instead of 49°, which is

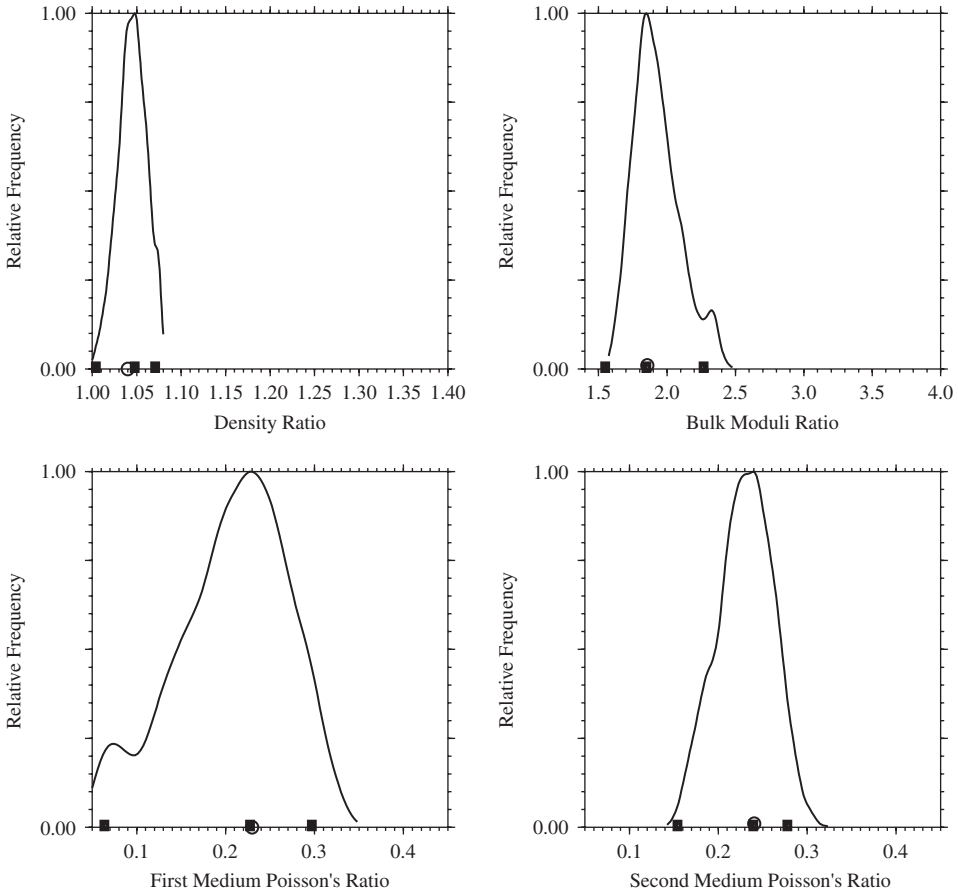

Fig. 9. Distribution functions of solutions for density ratio, bulk moduli ratio and Poisson's ratio of each layer for shale/limestone (gas) interface model used in inversion procedure. Solid square at peak value (mode) indicates the most likely parameters while squares on either sides show 90% confidence limits of the most likely parameters. Open circle in horizontal axis shows actual value of elastic parameters ($r_\rho = 1.04, r_k = 1.86, \sigma_1 = 0.23, \sigma_2 = 0.24$).

the critical angle for the shale/limestone (gas) model, results are not satisfactory (Fig. 10). The reason for that is the loss of the highly varying part of R_{pp} and R_{ps} data sets near critical angle of 49° (Fig. 5). The bootstrapping number was tested within 1000–10 000 repetitions. As solutions did not improve by choosing large numbers, the repetition was chosen to be 1000.

2. Conclusions

Joint inversion of AVA data for P and S-converted waves estimates the ratios of densities and bulk moduli (r_ρ and r_k), and Poisson's ratios (σ_1 and σ_2) for a two-layered horizontal model. The Zoeppritz equations, the physical model of this inversion, are designated as analytical for R_{pp} and R_{ps} and the partial derivatives of model parameters in the Jacobian matrix of the inversion procedure are taken analytically to get a better precision. Two models are tested in the inversion: shale/limestone and shale/limestone (gas) interface models. The parameters from the models are inverted even with having 5%, 7% and 10% random noise added to the data. Results are better when the lower layer contains gas (shale/limestone (gas) case). As the random noise is increased to 10%, unknown values are approximately estimated for all parameters. The joint use of P and S-converted wave reflections, instead of P reflections only, improves the inversion solutions significantly on a large scale. RFMs prove this result with elliptical closed contours around the true parameter pairs for the joint case. The contribution of the S reflections to the success of the inversion procedure is also seen in the partial derivative graphs with a significant change in values.

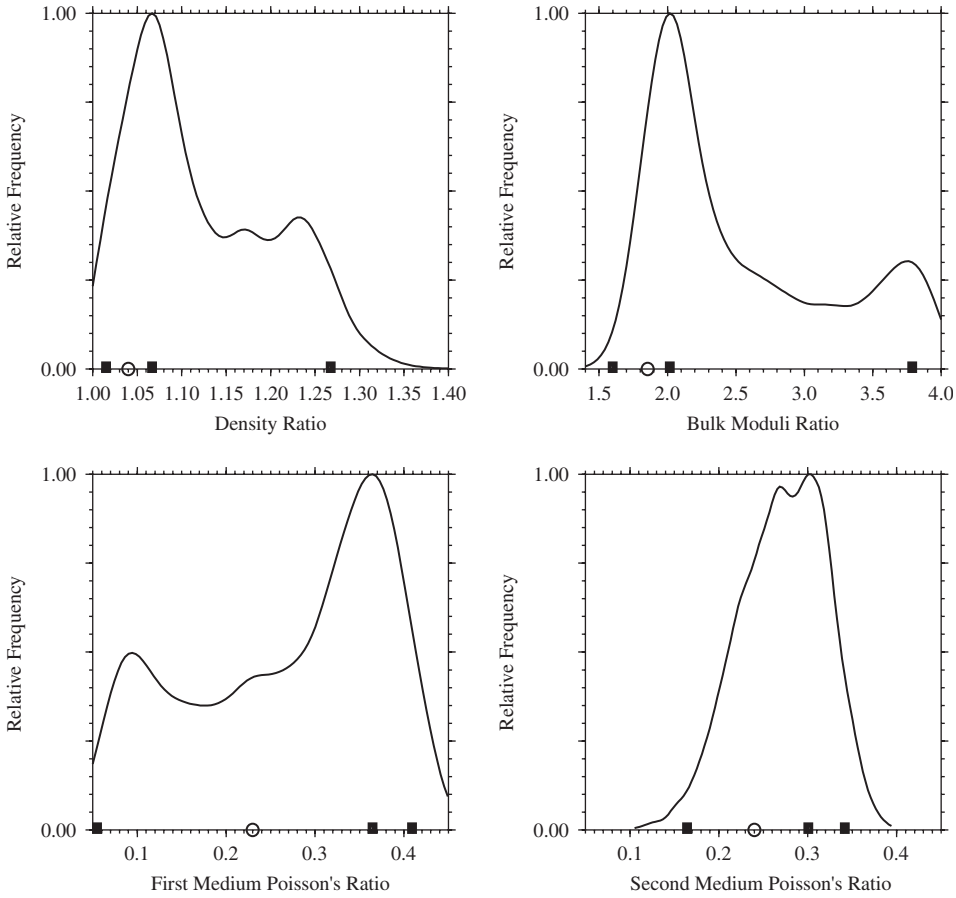

Fig. 10. Distribution functions of solutions for density ratio, bulk moduli ratio and Poisson's ratio of each layer for shale/limestone (gas) interface model evaluated from 1° to a smaller value of critical incidence angle (30°). Solid square at peak value (mode) indicates the most likely parameters while squares on either side show 90% confidence limits of the most likely parameters. Open circle in horizontal axis shows actual value of elastic parameters ($r_\rho = 1.04, r_k = 1.86, \sigma_1 = 0.23, \sigma_2 = 0.24$).

The bootstrapping method enhances results with repeating inversion procedure when the data have random noise. The evaluated maximum angle of incidence is important in the inversion and should be chosen as close as possible to the critical angle. During inversion the amplitude data, *P* and *S*-converted reflection amplitudes, are normalized to the values of the first angle, i.e., 1° (R_{pp} (1) and R_{ps} (1)). Because the analytic computation of the Jacobian derivatives from the Zoeppritz formulation cannot be calculated at normalized to 0° angle of incidence due to the uncertainty, reflections are normalized to the angle of 1°. This is different than many general AVO/AVA studies that use reflections normalized to zero angle of incidence. Originally, inversion results are more successful when using true amplitudes, i.e., without normalization. However, true amplitudes are generally needed to be accurate and these are not recovered easily. To overcome this problem, normalized amplitudes, i.e., *P* and *S*-converted reflection amplitude changes are used in this study. The inversion results are successful even with the normalized data.

Acknowledgments

I thank Dr. Emin Demirbağ for valuable discussions. Dr. Tuğrul Genç and Dr. Onur Tan helped me on the computational matters. I thank Dr. Ayşe Kaşlılar, Dr. Rengin Gök and Dr. Christopher Sorlien for manuscript editing. This study was partly supported by the İTÜ Research Project Funds.

Appendix

The linear equation system form of P and S-converted wave reflection coefficients (R_{pp} and R_{ps}) in terms of model parameters of this study ($r_\rho = \rho_2/\rho_1, r_k = \rho_2/\rho_1, \sigma_1$ and σ_2). R_{pp} and R_{ps} are derived from the classical form of the Zoeppritz equations by transforming P and S-converted wave velocities to the elastic constants. Because R_{pp}, R_{ps} and their partial derivatives to the model parameters are extracted analytically, their expressions could be obtained and easily implemented as Fortran code for the inversion technique of this study. In the formulas, $\theta_r(=\theta_1)$ and Φ_r indicate P and S-wave reflection angles while θ_t and Φ_t indicate$P$ and S-wave transmission angles. Because the incidence angle of P-wave is equal to the reflection angle of P-wave ($\theta_r = \theta_1$), in the equations θ_r is not used.

$$R_{pp} = \frac{a - b\left(\frac{c}{d}\right)}{e - f\left(\frac{c}{d}\right)}, \quad R_{ps} = \frac{\left(\frac{g}{h}\right)j + k}{\left(\frac{g}{h}\right)l - m},$$

$$a = \sin(2\theta_1) + \frac{\cos\theta_1}{\sin\phi_r}\cos(2\phi_r)\left[\frac{1-\sigma_1}{0,5-\sigma_1}\right]^{1/2} - \left(\frac{\cos\theta_t}{\sin\phi_r}\cos(2\phi_r)\left[\frac{1-\sigma_1}{0,5-\sigma_1}\right] + \sin(2\theta_t)\left[\frac{\rho_2}{\rho_1}\right]^{1/2} \times \left[\frac{k_2}{k_1}\right]^{1/2}\left[\frac{(1-\sigma_1)(1+\sigma_1)}{(1-\sigma_2)(1+\sigma_2)}\right]^{1/2}\left[\frac{1-2\sigma_2}{1+2\sigma_1}\right]\right)\left(\frac{\cos\theta_1\cot\phi_r - \sin\theta_1}{\cos\theta_t\cot\phi_r - \sin\theta_t}\right),$$

$$b = \cos(2\phi_r) + \frac{\cos(\theta_1)}{\sin(\phi_r)}\sin(2\phi_r)\left[\frac{0.5-\sigma_1}{1-\sigma_1}\right]^{1/2} - \left\{\frac{\cos\theta_t}{\sin\phi_r}\sin(2\phi_r)\left[\frac{0.5-\sigma_1}{1-\sigma_1}\right]^{1/2} + \cos(2\phi_t) \times \left[\frac{\rho_2}{\rho_1}\right]^{1/2}\left[\frac{k_2}{k_1}\right]^{1/2}\left[\frac{(1-\sigma_2)(1+\sigma_1)}{(1+\sigma_2)(1-\sigma_1)}\right]^{1/2}\right\}\left(\frac{\cos\theta_1\cot\phi_r - \sin\theta_1}{\cos\theta_t\cot\phi_r - \sin\theta_t}\right),$$

$$\frac{c}{d} = \frac{\left[\begin{array}{l}\frac{\sin\phi_t}{\sin\phi_r}\cos(2\phi_r)\left[\frac{1-\sigma_1}{0,5-\sigma_1}\right]^{1/2} - \cos(2\phi_t)\left[\frac{\rho_2}{\rho_1}\right]^{1/2}\left[\frac{k_2}{k_1}\right]^{1/2}\left[\frac{2(1-2\sigma_2)(1-\sigma_1)}{(1+\sigma_2)(1+\sigma_1)}\right]^{1/2}\left[\frac{1+\sigma_1}{1-2\sigma_1}\right] \\ \quad -\left\{\frac{\cos\theta_t}{\sin\phi_r}\cos(2\phi_r)\left[\frac{1-\sigma_1}{0,5-\sigma_1}\right]^{1/2} + \sin(2\theta_t)\left[\frac{\rho_2}{\rho_1}\right]^{1/2}\left[\frac{k_2}{k_1}\right]^{1/2}\left[\frac{(1-\sigma_1)(1+\sigma_1)}{(1-\sigma_2)(1+\sigma_2)}\right]^{1/2}\left[\frac{1-2\sigma_2}{1+2\sigma_1}\right]\right\}\left(\frac{\sin\phi_t\cot\phi_r + \cos\phi_t}{\cos\theta_t\cot\phi_r - \sin\theta_t}\right)\end{array}\right]}{\left[\begin{array}{l}-\frac{\sin\phi_t}{\sin\phi_r}\sin(2\phi_r)\left[\frac{0,5-\sigma_1}{1-\sigma_1}\right]^{1/2} - \sin(2\phi_t)\left[\frac{\rho_2}{\rho_1}\right]^{1/2}\left[\frac{k_2}{k_1}\right]^{1/2}\left[\frac{(1-2\sigma_2)(1+\sigma_1)}{2(1+\sigma_2)(1-\sigma_1)}\right]^{1/2} \\ \quad +\left[\frac{\cos\theta_t}{\sin\phi_r}\sin(2\phi_r)\left[\frac{0,5-\sigma_1}{1-\sigma_1}\right]^{1/2} + \cos(2\phi_t)\left[\frac{\sigma_2}{\sigma_1}\right]^{1/2}\left[\frac{k_2}{k_1}\right]^{1/2}\left[\frac{(1-\sigma_2)(1+\sigma_1)}{(1+\sigma_2)(1-\sigma_1)}\right]^{1/2}\right]\left(\frac{\sin\phi_t\cot\phi_r + \cos\phi_t}{\cos\theta_t\cot\phi_r - \sin\theta_t}\right)\end{array}\right]},$$

$$e = \sin(2\theta_1) + \frac{\cos\theta_1}{\sin\phi_r}\cos(2\phi_r)\left[\frac{1-\sigma_1}{0,5-\sigma_1}\right]^{1/2} - \left(\frac{\cos\theta_t}{\sin\phi_r}\cos(2\phi_r)\left[\frac{1-\sigma_1}{0,5-\sigma_1}\right] + \sin(2\theta_t)\left[\frac{\rho_2}{\rho_1}\right]^{1/2} \times \left[\frac{k_2}{k_1}\right]^{1/2}\left[\frac{(1-\sigma_1)(1+\sigma_1)}{(1-\sigma_2)(1+\sigma_2)}\right]^{1/2}\left[\frac{1-2\sigma_2}{1+2\sigma_1}\right]\right)\left(\frac{\cos\theta_1\cot\phi_r + \sin\theta_1}{\cos\theta_t\cot\phi_r - \sin\theta_t}\right),$$

$$f = -\cos(2\phi_r) + \frac{\cos(\theta_1)}{\sin(\phi_r)}\sin(2\phi_r)\left[\frac{0.5-\sigma_1}{1-\sigma_1}\right]^{1/2} - \left\{\frac{\cos\theta_t}{\sin\phi_r}\sin(2\phi_r)\left[\frac{0.5-\sigma_1}{1-\sigma_1}\right]^{1/2} + \cos(2\phi_t)\left[\frac{\rho_2}{\rho_1}\right]^{1/2} \times \left[\frac{k_2}{k_1}\right]^{1/2}\left[\frac{(1-\sigma_2)(1+\sigma_1)}{(1+\sigma_2)(1-\sigma_1)}\right]^{1/2}\right\}\left(\frac{\cos\theta_1\cot\phi_r - \sin\theta_1}{\cos\theta_t\cot\phi_r - \sin\theta_t}\right),$$

$$g = \frac{\sin\phi_t \tan\theta_1 - \cos\phi_t}{\cos\theta_t \tan\theta_1 + \sin\theta_t}\left[\frac{\cos\theta_t}{\cos\theta_1}\cos(2\phi_r) + \left[\frac{\rho_2}{\rho_1}\right]^{1/2}\left[\frac{k_2}{k_1}\right]^{1/2}\left[\frac{(1-\sigma_2)(1+\sigma_1)}{(1+\sigma_2)(1-\sigma_1)}\right]^{1/2}\cos(2\theta_t)\right]$$
$$-\left[\frac{\sin\phi_t}{\cos\theta_1}\cos(2\phi_r) + \left[\frac{\rho_2}{\rho_1}\right]^{1/2}\left[\frac{k_2}{k_1}\right]^{1/2}\left[\frac{(1-2\sigma_2)(1+\sigma_1)}{2(1+\sigma_2)(1-\sigma_1)}\right]\sin(2\phi_t)\right],$$

$$h = \frac{\sin\phi_t \tan\theta_1 - \cos\phi_t}{\cos\theta_t \tan\theta_1 + \sin\theta_t}\left[\left[\frac{\rho_2}{\rho_1}\right]^{1/2}\left[\frac{k_2}{k_1}\right]^{1/2}\left[\frac{(1-\sigma_1)(1+\sigma_1)}{(1-\sigma_2)(1-\sigma_2)}\right]^{1/2}\left[\frac{1-2\sigma_2}{1-2\sigma_1}\right]\sin(2\theta_t) - 2\cos\theta_t\sin\theta_1\right]$$
$$+\left[2\sin\phi_t\sin\theta_1 + \left[\frac{\rho_2}{\rho_1}\right]^{1/2}\left[\frac{k_2}{k_1}\right]^{1/2}\left[\frac{2(1-2\sigma_2)(1-\sigma_1)}{(1+\sigma_2)(1+\sigma_1)}\right]^{1/2}\left[\frac{1+\sigma_1}{1-2\sigma_1}\right]\cos(2\phi_t)\right],$$

$$j = \left\{-\frac{2\sin\theta_1}{\cos\theta_t \tan\theta_1 + \sin\theta_t}\left[\left[\frac{\rho_2}{\rho_1}\right]^{1/2}\left[\frac{k_2}{k_1}\right]^{1/2}\left[\frac{(1-\sigma_1)(1+\sigma_1)}{(1-\sigma_2)(1+\sigma_2)}\right]\left[\frac{1-2\sigma_2}{1-2\sigma_1}\right]\sin(2\theta_t) - 2\cos\theta_t\sin\theta_1\right]\right\},$$

$$k = \left\{\frac{2\sin\theta_1}{\cos\theta_t \tan\theta_1 + \sin\theta_t}\left[\frac{\cos\theta_t}{\cos\theta_1}\cos(2\theta_1) + \left[\frac{\rho_2}{\rho_1}\right]^{1/2}\right.\right.$$
$$\left.\left.\times\left[\frac{k_2}{k_2}\right]^{1/2}\left[\frac{(1-\sigma_2)(1+\sigma_1)}{(1+\sigma_2)(1-\sigma_1)}\right]^{1/2}\cos(2\phi_t)\right]\right\} - 2\cos(2\phi_r),$$

$$l = \frac{\sin\phi_r \tan\theta_1 + \cos\phi_r}{\cos\theta_t \tan\theta_1 + \sin\theta_t}\left\{\left[\frac{\rho_2}{\rho_1}\right]^{1/2}\left[\frac{k_2}{k_1}\right]^{1/2}\right.$$
$$\left.\times\left[\frac{(1-\sigma_1)(1+\sigma_1)}{(1-\sigma_2)(1+\sigma_2)}\right]^{1/2}\left[\frac{1-2\sigma_2}{1-2\sigma_1}\right]\sin(2\theta_t) - 2\cos\theta_t\sin\theta_1\right\}$$
$$+2\sin\phi_r\sin\theta_1 + \left[\frac{1-\sigma_1}{0.5-\sigma_1}\right]^{1/2}\cos(2\phi_r),$$

$$m = \frac{\sin\phi_r \tan\theta_1 + \cos\phi_r}{\cos\theta_t \tan\theta_1 + \sin\theta_t}\left\{\frac{\cos\theta_t}{\cos\theta_1}\cos(2\theta_1) + \left[\frac{\rho_2}{\rho_1}\right]^{1/2}\right.$$
$$\left.\times\left[\frac{k_2}{k_1}\right]^{1/2}\left[\frac{(1-\sigma_2)(1+\sigma_1)}{(1+\sigma_2)(1-\sigma_1)}\right]^{1/2}\cos(2\phi_t)\right\}$$
$$-\left[\frac{\sin\phi_r}{\cos\theta_1}\cos(2\phi_r) - \left(\frac{0.5-\sigma_1}{1-\sigma_1}\right)^{1/2}\sin(2\phi_r)\right].$$

References

Aki, K., Richards, P.G., 2002. Quantitative Seismology. University Science Books, Sausalito, CA, 700pp.

Backus, M.M., 1987. Amplitude versus offset: a review. In: Proceedings of the 57th International Meeting of the Society of Exploration Geophysics, New Orleans, LA, pp. 359–364.

Berkhout, A.J., 1987. Applied Seismic Wave Theory. Elsevier Science Publication, New York, 468pp.

Bortfeld, R., 1961. Approximations to the reflection and transmission coefficients of plane longitudinal and tranverse waves. Geophysical Prospecting 9, 485–502.

Buland, A., Landrø, M., Andersen, M., Dahl, T., 1996. AVO inversion of Troll field data. Geophysics 61, 1589–1602.

Buland, A., Landrø, M., 2001. The impact of common-offset migration on porosity estimation by AVO inversion. Geophysics 66, 755–762.

Buland, A., Kolbjornsen, O., More, H., 2003. Rapid spatially coupled AVO inversion in the Fourier domain. Geophysics 68, 824–836.

Buland, A., More, H., 2003. Joint AVO inversion, wavelet estimation and noise-level estimation using a spatially coupled hierarchical Bayesian model. Geophysical Prospecting 51, 531–550.

Carazzone, J.J., Srnka, L.J., 1993. Elastic inversion of Gulf of Mexico data. In: Castagna, J.P., Backus, M.M. (Eds.), Offset-Dependent Reflectivity-Theory and Practice of AVO Analysis, Investigations in Geophysics, vol. 8. Society of Exploration Geophysics, Tulsa, OK, pp. 303–313.

Dahl, T., Ursin, B., 1992. Non-linear AVO inversion for a stack of anelastic layers. Geophysical Prospecting 40, 243–265.

Demirbağ, E., Çoruh, C., Costain, J.K., 1993. Inversion of P-Wave AVO. In: Castagna, J.P., Backus, M.M. (Eds.), Offset-Dependent Reflectivity-Theory and Practice of AVO Analysis, Investigations in Geophysics, vol. 8. Society of Exploration Geophysics, Tulsa, OK, pp. 287–302.

Dey-Sarkar, S.K., Svatek, S.V., 1993. Prestack analysis—an integrated approach for seismic interpretation in classics basins. In: Castagna, J.P., Backus, M.M. (Eds.), Offset-Dependent Reflectivity—Theory and Practice of AVO Analysis, Investigations in Geophysics, vol. 8. Society of Exploration Geophysics, Tulsa, OK, pp. 57–77.

Domenico, S.N., 1977. Elastic properties of unconsolidated porous sand reservoirs. Geophysics 42, 1339–1369.

Efron, B., Gong, G., 1983. A leisurely look at the bootstrap, the jackknife, and cross-validation. American Statistician 37, 36–48.

Efron, B., Tibshirani, R.J., 1993. An Introduction to the Bootstrapping. Chapman & Hall, New York, 436pp.

Goodway, B., Chen, T., Downton, J., 1997. Improved AVO fluid detection and lithology discrimination using Lame petrophysical parameters; "$\lambda\rho$", "$\mu\rho$", & "λ/μ fluid stack", from P and S inversions. In: Proceedings of the 67th International Meeting of the Society of Exploration Geophysics, Dallas, TX, pp. 183–186.

Larsen, J.A., 1999. AVO inversion by simultaneous P–P and P–S inversion. M.Sc. Thesis, The University of Calgary, 124pp.

Lavaud, B., Kabir, N., Chavent, G., 1999. Pushing AVO inversion beyond linearized approximation. Journal of Seismic Exploration 8, 279–302.

Lines, L.R., Treitel, S., 1984. Tutorial: a review of least squares inversion and its application to geophysical problems. Geophysical Prospecting 32, 159–186.

Mahob, P.N., Castagna, J.P., Young, R.A., 1999. AVO inversion of a Gulf of Mexico bright spot—a case study. Geophysics 64, 1480–1491.

Margrave, G.F., Stewart, R.R., Larsen, J.A., 2001. Joint PP and PS seismic inversion. The Leading Edge 20, 1048–1052.

Ostrander, W.J., 1984. Plane-wave reflection coefficients for gas sands at nonnormal angles of incidence. Geophysics 49, 1637–1648.

Pigott, J.D., Shrestha, R.K., Warwick, R.A., 1989. Young modulus from AVO inversion. In: Proceedings of the 59th International Meeting of the Society of Exploration Geophysics, vol. 2, Dallas, TX, pp. 832–835.

Riedel, M., Dosso, S.E., Beran, L., 2003. Uncertainty estimation for amplitude variation with offset (AVO) inversion. Geophysics 68, 1485–1496.

Rutherford, S.R., Williams, R.H., 1989. Amplitude-versus-offset variations in gas sands. Geophysics 54, 680–688.

Sheriff, R.E., Geldart, L.P., 1995. Exploration Seismology. Cambridge University Press, New York, 592pp.

Shuey, R.T., 1985. A simplification of the Zoeppritz equations. Geophysics 50, 609–614.

Stewart, R.R., Zhang, Q., Guthoff, F., 1995. Relationships among elastic-wave values: Rpp, Rps, Rss, Vp, Vs, k, σ and ρ. The CREWES Project Research Report # 7, The University of Calgary, 9pp.

Wang, Y., 1999. Simultaneous inversion for model geometry and elastic parameters. Geophysics 64, 182–190.

Zoeppritz, K., 1919. On reflection and propagation of seismic waves. Gottinger Nachrichten I, 66–84.